MATERIALS PHYSICS AND MECHANICS RESEACH ARTICLE

Submitted: February 1, 2024 **Revised: March 6, 2024** **Accepted: June 10, 2024**

Interaction of two circular holes in an infinite plate by body force method

S.M. Badiger [1] ✉, **D.S. Ramakrishna** [2]

[1] M.S. Ramaiah University of Applied Sciences, Bengaluru, India

[2] Jawaharlal Nehru National College of Engineering, Shivamogga, India

✉ krishnabadiger@yahoo.com

ABSTRACT

The body force method is used to perform stress analysis around two circular holes with equal and different sizes in an infinite plate subjected to uni-axial loading. The elasticity solution for a point force in an infinite plate is used as the fundamental solution. Traction free boundary conditions are satisfied at the midpoint of segments. Stress concentration factors obtained by body force method are compared with the results available in the literature. It is noted that accurate results are obtained with a small number of segments of the discontinuity. The body force method is simple, yet robust method useful in performing stress analysis of bodies with discontinuities.

KEYWORDS

two unequal circular holes • body force method • stress concentration factor • infinite plate • uni-axial loading

Acknowledgements. *The authors would like to thank Mahesh Varpe and Kiran Hubballi for their generosity and permitting to use computing facility. No external funding was received for this study.*

Citation: Badiger SM, Ramakrishna DS. Interaction of two circular holes in an infinite plate by body force method. *Materials Physics and Mechanics*. 2024;52(3): 96–107.
http://dx.doi.org/10.18149/MPM.5232024_10

Introduction

In many structural applications, multiple holes are used to achieve required functionality. In applications where multiple holes exist, interaction of holes and its effect on stress concentration factor becomes important consideration to a design engineer. In this regard, interaction of two circular holes (Fig. 1) has attracted attention of many researchers. Ling [1] employed bipolar coordinates, taking advantage of double symmetry solved the problem of two equal circular holes with all around tension, longitudinal tension and transverse tension cases. Davies [2] obtained approximate solutions to the problem of two unequal circular holes employing complex variable technique. The method employed is restricted because of collocation on one of the boundaries. Haddon [3] obtained closed form solution in series form, using complex variable technique for the case of two unequal circular holes. Stress concentration factor (SCF) was computed for the case of angle α (angle between line connecting centers of the holes and the far field uniform tension) equal to 0°, 90° and 45°. Salerno [4] employed complex variable technique, Schwartz Alternating Method with successive approximations to obtain stress distribution around two unequal circular holes under equal biaxial stresses. Miyata [5] investigated stresses around two circular holes in an infinite plate subjected to biaxial tension using complex variable method with method of successive approximations. Miyata presented numerical results for uniaxial longitudinal tension and transverse

tension. In a finite plate, Erickson [6] used 2D photoelasticity and obtained the optimum size and locations of multiple ancillary holes near central hole. Iwaki [7] used bipolar coordinates and obtained explicit solution for stresses around two unequal circular holes subjected to far-field uniform tension, uniform internal pressure and uniform shearing stresses along a hole. Horii [8] used method of pseudotractions and obtained SCF around (a) two circular holes (b) three circular holes in a row (c) infinite row of equal circular holes in an infinite plate under uniaxial longitudinal tension and transverse tension. This method was also used to obtain stress intensity factor (SIF) in the case of (a) two cracks and (b) infinite rows collinear/parallel cracks. Duan [9] used integral equation technique to study (a) hole to edge dislocation interaction (b) hole to hole interaction (c) hole to free boundary interaction. Chiang [10] obtained SCF around two unequal circular holes using a numerical method which resembles the method of fundamental solutions for longitudinal tension and transverse tension cases. To study the interaction between existing major holes (three holes) and the "defense" hole system (addition of two, four smaller holes) in a plate under uniaxial tension, Meguid [11] conducted analytical, finite element analysis and photoelastic tests. For the problem of two circular holes in plane stress and uniform internal pressure inside the holes, Hoang [12] derived explicit expression for the stress distribution near holes. Ukadgaonker [13] investigated SCF around two unequal circular holes in an infinite plate under longitudinal tension and transverse tension cases using Schwarz Alternating Method. Kuo [14] studied degenerate scale problem of the infinite plane containing two equal circular holes. Zeng [15] obtained optimal shape of two closely spaced holes under biaxial loading using differential-evolution algorithm to compute coefficients of mapping function. Mohan [16] performed stress analysis of rectangular plates with two symmetrical circular holes under uniaxial tension for two material types (PLA, PLA/15%carbon) and compared results from experiments and finite element method. Gandilyan [17] solved the problem of two equal holes in a plane subjected to biaxial tension using bipolar coordinates and series expansion taking into account the effects of surface elasticity. Patel [18] obtained expression for tangential stress concentration factor around an elliptical hole in a large rectangular plate subjected to linearly varying in-plane loading on two opposite edges. Yang [19] designed 5 crack models and studied the propensity of forming the hook pattern. Simulations were carried out for the two borehole case employing the 5 models using the T-stress at the crack tip and the incremental crack growth method is adopted to simulate the crack propagation paths. Ma [20] proposed solution to elastoplastic problem of an infinite medium containing two equal circular holes. The preconditions followed are the two plastic regions formed are disconnected with each other, and each plastic region can completely surround each hole. The influences of the separation distance between the two holes and the loads on the plastic regions were analyzed. Maksymovych [21] studied stress concentration at closely placed holes in wing bearing area of anisotropic plate. Asymptotic formula for stresses near holes was employed, implementation of the approach was carried out using Boundary Integral equation method and method of least squares.

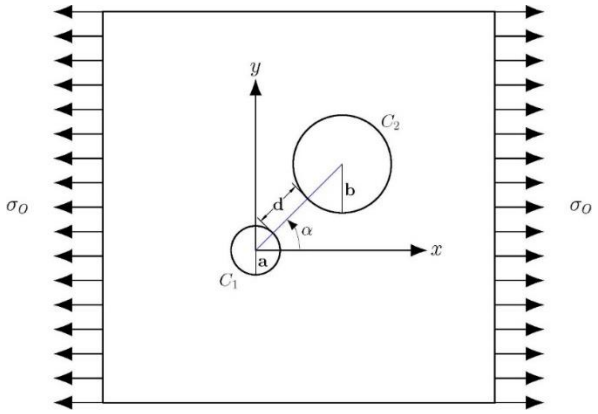

Fig. 1. Two circular holes in an infinite plate under uniaxial tension

The body force method has been used in the present work to examine the interaction of two circular holes in isotropic infinite plate under uni-axial tension. Ratio of diameters ($\boldsymbol{b/a}$) is varied from 1 to 10, ratio of distance between holes $\boldsymbol{a}$ to diameter, ($\boldsymbol{d/a}$) is varied from 0.4 to 10 and angle ($\boldsymbol{\alpha}$) between the line joining two centers and direction of uniaxial tension is varied from 0° to 90°. In the next section description of body force method is provided. In the "Body force method applied to two circular holes" section, application of body force method is discussed. In the "Numerical results and Discussion" section, numerical results along with plots, discussion and comparison with data from literature are presented followed by concluding remarks in the "Conclusions" section.

Body force method

Nisitani [22–24] originally proposed the body force method (BFM) which is a boundary integral type approach helpful in performing stress analysis. Detailed account of BFM can be found in [25]. In using BFM, actual discontinuity (for e.g. circular hole) present in an infinite plate is visualized as an imaginary condition, i.e. infinite plate with a hole is treated as a plate without hole. The hole is visualized as an imaginary curve divided into M number of segments forming its boundary. In order to achieve traction free boundary condition at the boundary of the imaginary curve, at the midpoints of segments on its periphery, body force densities (ρ_{xi}, ρ_{yi}) are applied. Influence coefficients are computed from the equations of stress field in an infinite plate due to a point force and the boundary conditions of traction free at the midpoint of each segment are applied and body force densities are obtained. At each given point in the plate, stress produced is computed by a linear combination of the body force densities.

The stresses at location (x, y) in an infinite plate, due to concentrated point force $\boldsymbol{X}$ and $\boldsymbol{Y}$ acting at (ξ, η) are as follows.

$$\sigma_x^X = -F\, l\,\{(3+\nu)l^2 + (1-\nu)m^2\}\,X, \tag{1}$$

$$\sigma_y^X = F\, l\,\{(1-\nu)l^2 - (1+3\nu)m^2\}\,X, \tag{2}$$

$$\tau_{xy}^X = -F\, m\,\{(3+\nu)l^2 + (1-\nu)m^2\}\,X, \tag{3}$$

and

$$\sigma_x^Y = -F\, m\,\{(1+3\nu)l^2 - (1-\nu)m^2\}\,Y, \tag{4}$$

$$\sigma_y^Y = -F\, m\,\{(1-\nu)l^2 + (3+\nu)m^2\}\, Y, \tag{5}$$
$$\tau_{xy}^Y = -F\, l\,\{(1-\nu)l^2 + (3+\nu)m^2\}\, Y, \tag{6}$$

where

$$l = \frac{x-\xi}{y}, \tag{7}$$
$$m = \frac{y-\eta}{y}, \tag{8}$$
$$F = \frac{1}{4\pi y(l^2+m^2)^2}. \tag{9}$$

The effect of point force $\boldsymbol{X}$ or $\boldsymbol{Y}$ applied at (ξ, η) are computed from stress fields and these form the influence coefficients. As the relations $-d\xi = a\sin\theta\, d\theta$ and $d\eta = b\cos\theta\, d\theta$ prevail along the ellipse $(\xi = a\cos\theta\,, \eta = b\sin\theta)$, the coefficients can be expressed as:

$$\sigma_{xM}^{XN} = \int_N \sigma_x^X(\xi,\eta,x,y)\; b\;\cos\theta\; d\theta\; at\; X = 1, \tag{10}$$
$$\sigma_{yM}^{XN} = \int_N \sigma_y^X(\xi,\eta,x,y)\; b\;\cos\theta\; d\theta\; at\; X = 1, \tag{11}$$
$$\tau_{xyM}^{XN} = \int_N \tau_{xy}^X(\xi,\eta,x,y)\; b\;\cos\theta\; d\theta\; at\; X = 1, \tag{12}$$

and

$$\sigma_{xM}^{YN} = \int_N \sigma_x^Y(\xi,\eta,x,y)\; a\;\sin\theta\; d\theta\; at\; Y = 1, \tag{13}$$
$$\sigma_{yM}^{YN} = \int_N \sigma_y^Y(\xi,\eta,x,y)\; a\;\sin\theta\; d\theta\; at\; Y = 1, \tag{14}$$
$$\tau_{xyM}^{YN} = \int_N \tau_{xy}^Y(\xi,\eta,x,y)\; a\;\sin\theta\; d\theta\; at\; Y = 1, \tag{15}$$

where $\int_N$ represents integration of the N-th interval.

The Influence Coefficients σ_{xM}^{XN}, σ_{xM}^{YN}, σ_{yM}^{XN}, σ_{yM}^{YN}, τ_{xyM}^{XN}, τ_{xyM}^{YN} are the stresses at the mid-point of the M-th interval due to a body force on the N-th interval having unit body force densities ($\rho_x = 1$ or $\rho_y = 1$).

Applying the boundary conditions which result in stress-free midpoints for each interval lead to:

$$\sum_{N=1}^{MM}\rho_{xN}\left(\sigma_{xM}^{XN}\cos\varphi_M + \tau_{xyM}^{XN}\sin\varphi_M\right) + \sum_{N=1}^{MM}\rho_{yN}\left(\sigma_{xM}^{YN}\cos\varphi_M + \tau_{xyM}^{YN}\sin\varphi_M\right) = -\sigma_0\cos\varphi_M, \tag{16}$$
$$\sum_{N=1}^{MM}\rho_{xN}\left(\tau_{xyM}^{XN}\cos\varphi_M + \sigma_{yM}^{XN}\sin\varphi_M\right) + \sum_{N=1}^{MM}\rho_{yN}\left(\tau_{xyM}^{YN}\cos\varphi_M + \sigma_{yM}^{YN}\sin\varphi_M\right) = 0, \tag{17}$$

where ρ_{xN}, ρ_{yN} represent body force densities acting on the N-th interval along x and y direction respectively, σ_0 stress at infinity along x-direction and φ_M represents the angle between the x-axis and the ellipse's normal at the midpoint of the M-th interval: $\varphi_M = \tan^{-1}\left(\frac{a}{b}\tan\theta_M\right)$. Equations (16) and (17) results in $2M$ linear equations in $2M$ unknowns ρ_{xN}, ρ_{yN}.

A set of linear equations result from Eqs. (16) and (17) in matrix form is $\boldsymbol{Ax} = \boldsymbol{b}$, where $\boldsymbol{A}$ is a square matrix (size $2M \times 2M$) known as influence coefficient matrix (ICM) due to terms inside the brackets, $\boldsymbol{x}$ is body force density column vector and column vector $\boldsymbol{b}$ is the right hand side of Eqs. (16) and (17) representing traction due to applied uni-axial far field load.

The linear combination of the influence coefficients and body force densities at arbitrary point $Q(x, y)$ in an infinite plate is employed to calculate the stresses at $Q(x, y)$.

$$\sigma_x = \sum_{N=1}^{MM}\left(\rho_{xN}\sigma_{xP}^{XN} + \rho_{yN}\sigma_{xP}^{YN}\right) + \sigma_0, \tag{18}$$
$$\sigma_y = \sum_{N=1}^{MM}\left(\rho_{xN}\sigma_{yP}^{XN} + \rho_{yN}\sigma_{yP}^{YN}\right), \tag{19}$$
$$\tau_{xy} = \sum_{N=1}^{MM}\left(\rho_{xN}\tau_{xyP}^{XN} + \rho_{yN}\tau_{xyP}^{YN}\right). \tag{20}$$

Radial, hoop and shear stresses are computed using appropriate stress transformation.

Body force method applied to two circular holes

Two circular holes are divided into 4 segments, at the midpoint of each segments, body force densities (ρ_{xi}, ρ_{yi}) are applied. This arrangement is shown in Fig. 2. Influence coefficient matrix (ICM) takes the following form:

$$A = \begin{bmatrix} A_{11} & A_{12} \\ A_{21} & A_{22} \end{bmatrix}, \tag{21}$$

where A_{11} is the ICM (obtained from Eqs. (16) and (17) of circular hole C_1 due to body force densities ((ρ_{x1}, ρ_{y1}) to (ρ_{x4}, ρ_{y4})) applied on the segments of circular hole C_1. A_{12} is the ICM (obtained from Eqs. (16) and (17)) of circular hole C_1 due to body force densities ((ρ_{x5}, ρ_{y5}) to (ρ_{x8}, ρ_{y8})) applied on the segments of circular hole C_2. A_{21} is the ICM (obtained from Eqs. (16) and (17)) of circular hole C_2 due to body force densities ((ρ_{x1}, ρ_{y1}) to (ρ_{x4}, ρ_{y4})) applied on the segments of circular hole C_1. A_{22} is the ICM (obtained from Eqs. (16) and (17)) of circular hole C_2 due to body force densities ((ρ_{x5}, ρ_{y5}) to (ρ_{x8}, ρ_{y8})) applied on the segments of circular hole C_2. The body force density vector and traction vector on each segment due to applied uni-axial load takes the following form:

$$\boldsymbol{x}^T = [\rho_{x1} \quad \rho_{y1} \quad \rho_{x2} \quad \rho_{y2} \quad \rho_{x3} \quad \rho_{y3} \quad \rho_{x4} \quad \rho_{y4} \quad \rho_{x5} \quad \rho_{y5} \quad \rho_{x6} \quad \rho_{y6} \quad \rho_{x7} \quad \rho_{y7} \quad \rho_{x8} \quad \rho_{y8}] \tag{22}$$

$$\boldsymbol{b}^T = [-\sigma_0 \cos\varphi_1 \quad 0 \quad -\sigma_0 \cos\varphi_2 \quad 0 \quad -\sigma_0 \cos\varphi_3 \quad 0 \quad -\sigma_0 \cos\varphi_4 \quad 0 \quad -\sigma_0 \cos\varphi_5 \quad 0 \quad -\sigma_0 \cos\varphi_6 \quad 0 \quad -\sigma_0 \cos\varphi_7 \quad 0 \quad -\sigma_0 \cos\varphi_8 \quad 0] \tag{23}$$

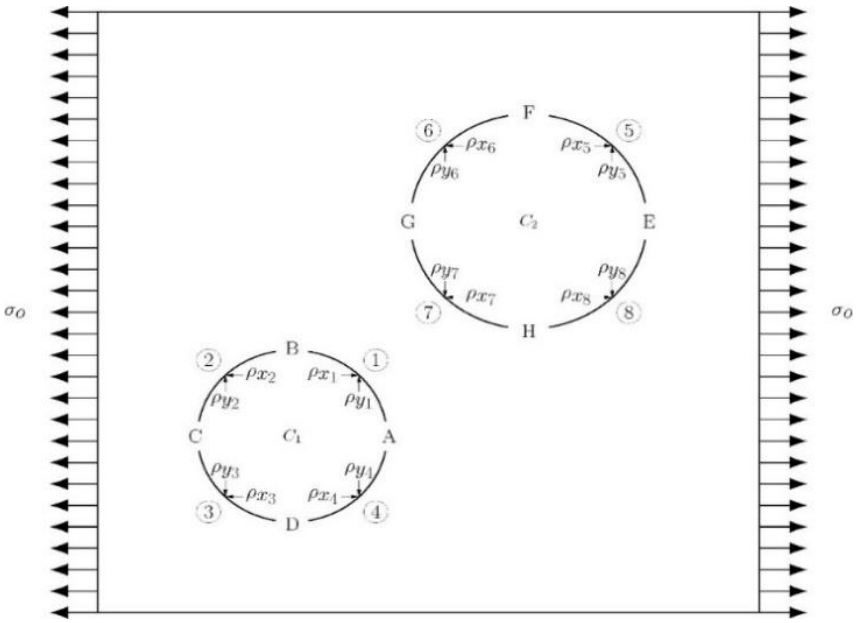

Fig. 2. An infinite plate under uni-axial tension with body force densities (ρ_{xi}, ρ_{yi}) applied at the mid-points of 4 segments of the two circular holes

Location of circular hole C_1 is fixed with center at $(0,0)$ and radius $a = 1$ is held constant, circular hole C_2 with center at (x_{c_2}, y_{c_2}) and radius b is varied. Values of radius b are varied from 1 to 10. Center to center distance l is related to radii of circular holes using the relation $l = a + d + b$. The values of l are chosen such that the ratio $^d/_a$ varies from 0.4 to 10. Angle α is varied from 0° to 90°. Both circular holes (C_1, C_2) are divided into 4 segments.

Numerical results and Discussion

A geometric configuration is first chosen (values of a, b, d, α, σ_o), Cartesian stresses are then computed (using Eqs. (18)–(20)) in the vicinity of the circular holes. Using stress transformation relationships, radial, hoop and shear stresses are computed. Hoop stress is extrapolated on the boundaries of the holes. Maximum value of hoop stress (occurring on the boundary of either of the holes) is identified and stress concentration factor (SCF) is computed. Figure 3 shows hoop stress variation along the boundary of holes (C_1, C_2) for configuration a = 1 mm, $\sigma_o = 1$ MPa and $\alpha = 45°$. Hoop stress varies in sinusoidal form on the hole boundary. SCF is computed for various values of b, d, α with uni-axial far field stress $\sigma_o = 1$ MPa and plots drawn are shown in Figs. 4–9.

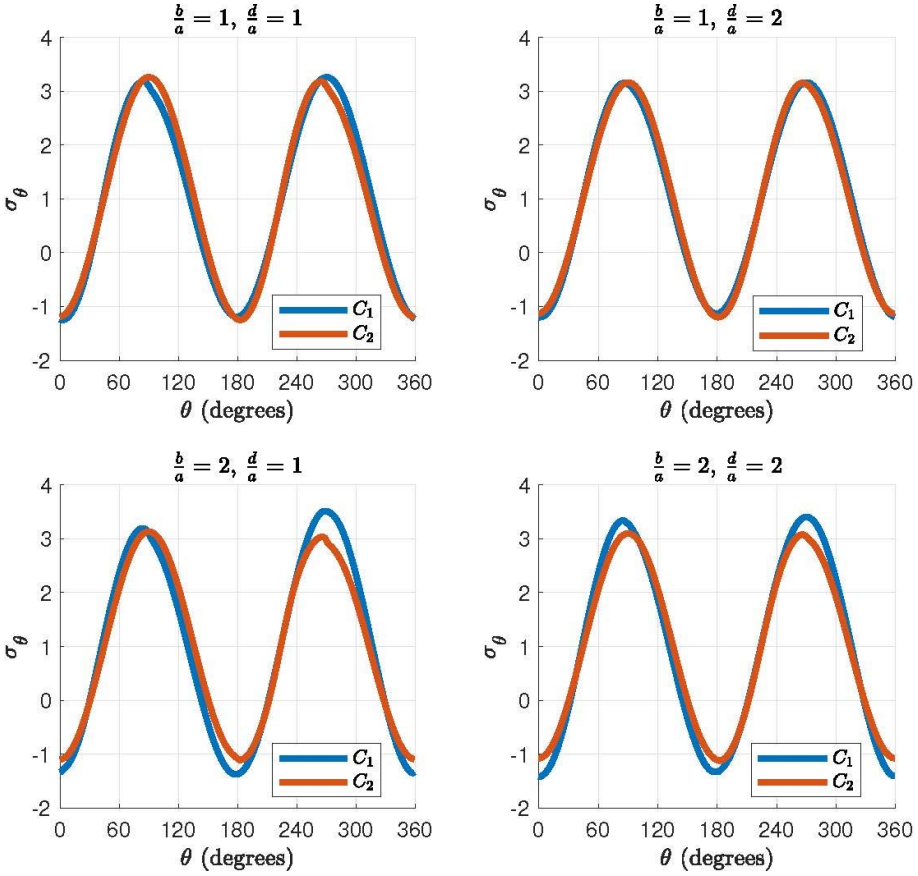

Fig. 3. Hoop stress variation on the hole boundary (C_1, C_2) for angle $\alpha = 45°$

Figure 4 shows plots of variation of SCF with angle α. These plots are generated at fixed values of ratio b/a and the individual curves correspond to a particular value of the ratio d/a as shown in the legend. The value of SCF remains well below 2.65 when two circular holes are equal in diameter, located farthest away from each other irrespective of the angle α. The value of SCF remains close to 3.0 when $b \geq 2a$ and angle α does not exceeds 30°. Maximum value of SCF shifts from 78° to 90° with increase in ratio b/a and shortest hole distance.

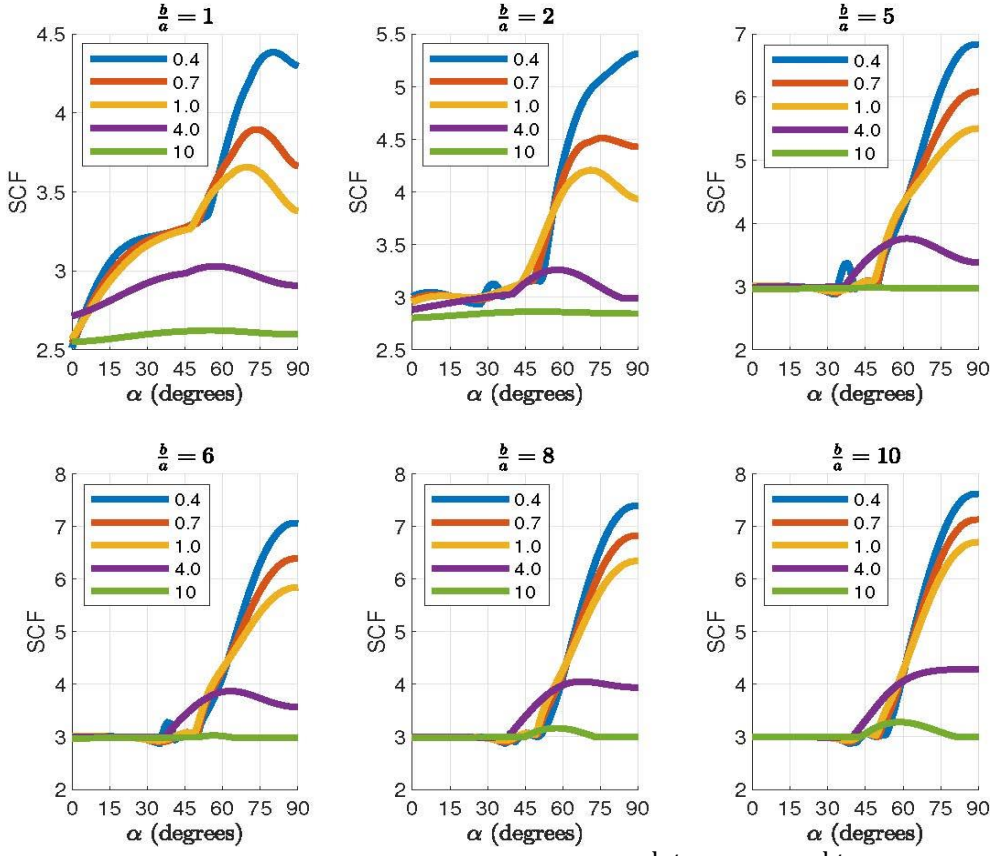

Fig. 4. Stress concentration factor variation with angle α for fixed $^{b}/_{a}$. The ratio $^{d}/_{a}$ varies from 0.4 to 10

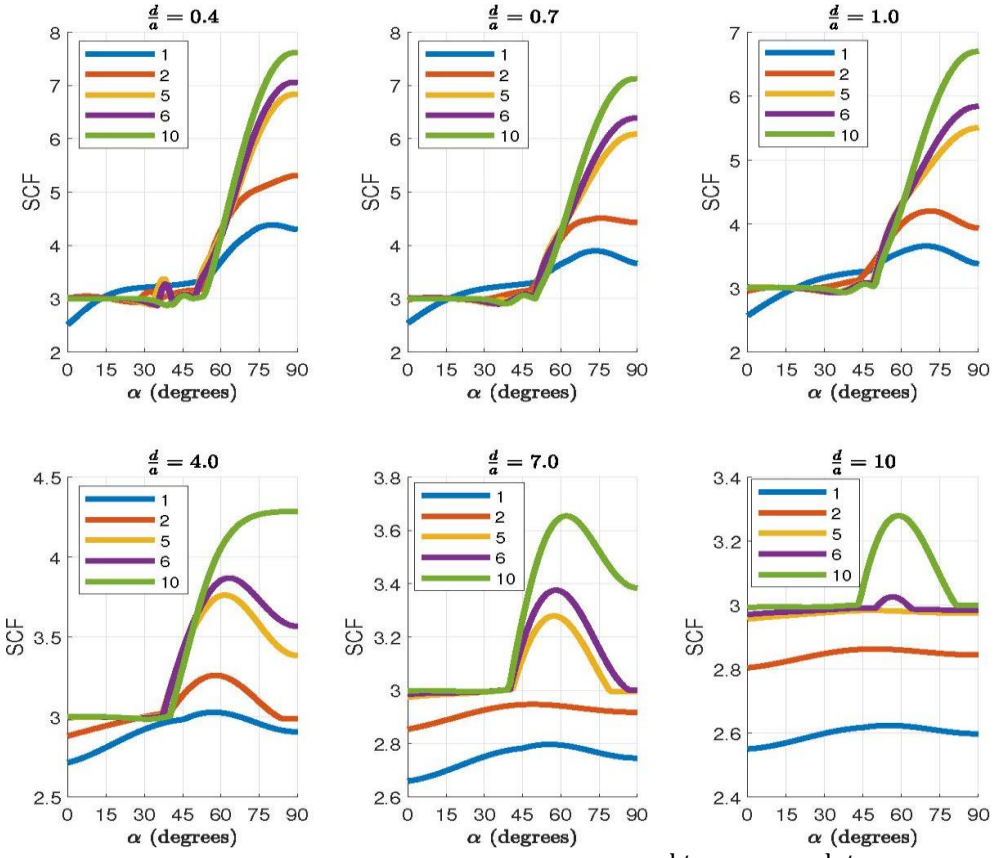

Fig. 5. Stress concentration factor variation with angle α for fixed $^{d}/_{a}$. The ratio $^{b}/_{a}$ varies from 1 to 10

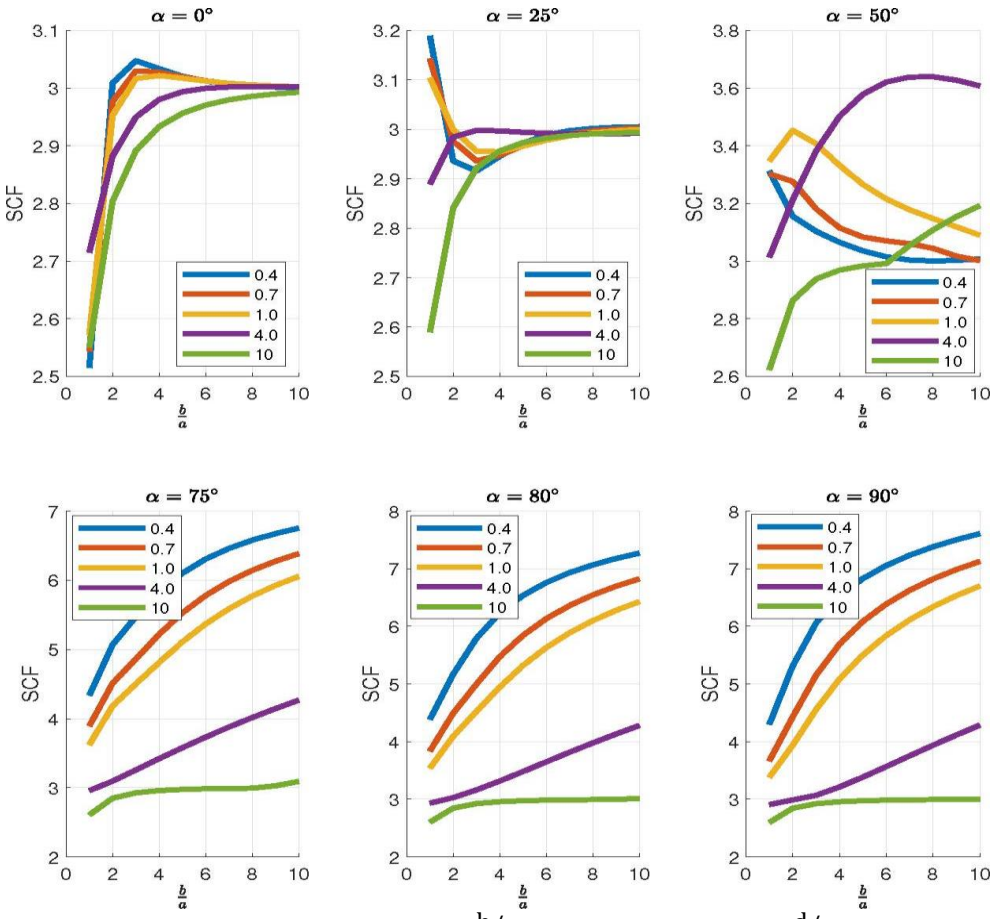

Fig. 6. Stress concentration factor variation with $^{b}/_{a}$ for fixed angle α. Ratio $^{d}/_{a}$ varies from 0.4 to 10

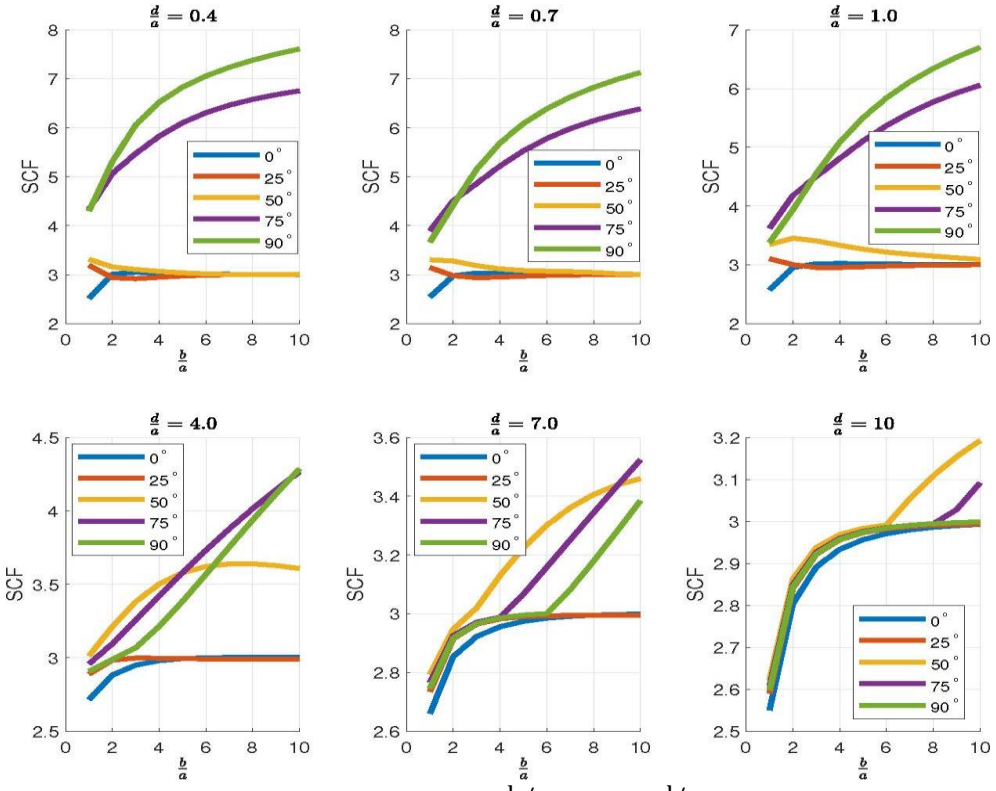

Fig. 7. Stress concentration factor variation with $^{b}/_{a}$ for fixed $^{d}/_{a}$. Angle α varies from 0° to 90°

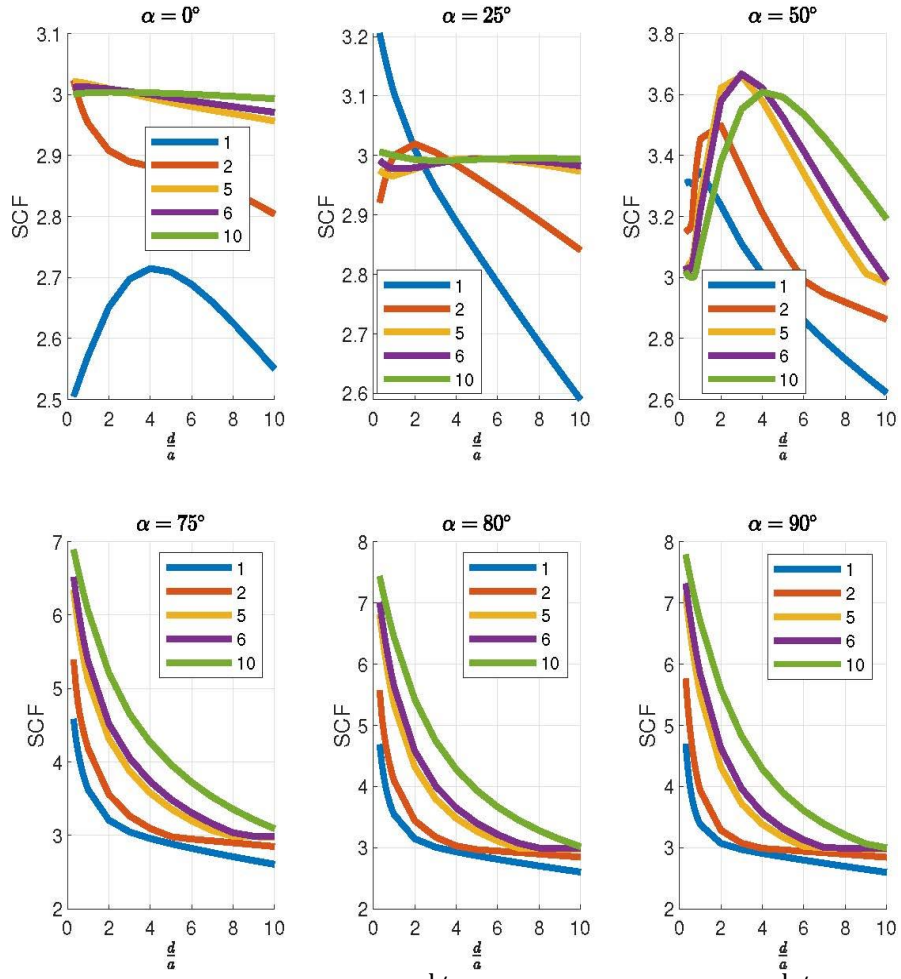

Fig. 8. Stress concentration factor variation with $^{d}/_{a}$ for fixed angle α. The ratio $^{b}/_{a}$ varies from 1 to 10

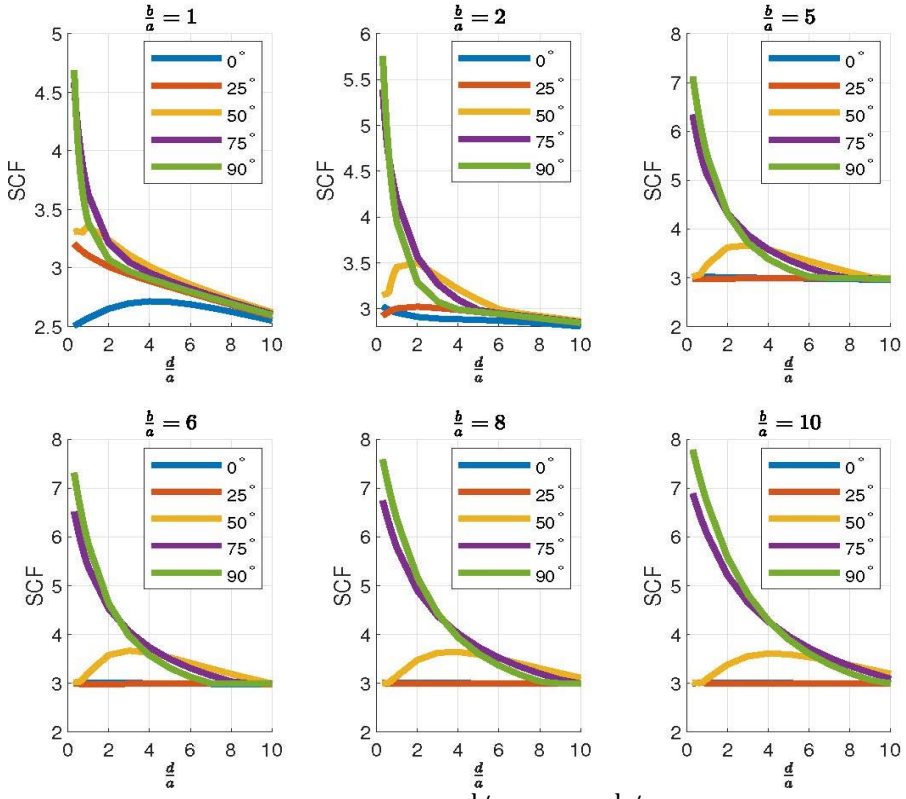

Fig. 9. Stress concentration factor variation with $^{d}/_{a}$ for fixed $^{b}/_{a}$. Angle α varies from 0° to 90°

Figure 5 shows plots of variation of SCF with angle α. These plots are generated at fixed values of ratio $^{d}/_{a}$ and the individual curves correspond to a particular value of the ratio $^{b}/_{a}$ as shown in the legend. With value of angle α from 35° to 55°, SCF increases monotonically for shorter center distances.

Figure 6 shows plots of variation of SCF with ratio $^{b}/_{a}$. These plots are generated at fixed values of angle α and the individual curves correspond to a particular value of the ratio $^{d}/_{a}$ as shown in the legend. With value of angle $\alpha \geq 55°$, SCF increases monotonically for shorter center distances.

Figure 7 shows plots of variation of SCF with ratio $^{b}/_{a}$. These plots are generated at fixed values of ratio $^{d}/_{a}$ and the individual curves correspond to a particular value of angle α as shown in the legend. The value of SCF remains below 3 for $b \leq 6a$ irrespective of the angle α.

Figure 8 shows plots of variation of SCF with ratio $^{d}/_{a}$. These plots are generated at fixed values of angle α and the individual curves correspond to a particular value of the ratio $^{b}/_{a}$ as shown in the legend. The lower three subplots confirm "With value of angle $\alpha \geq 55°$, SCF increases monotonically for shorter center distances".

Figure 9 shows plots of variation of SCF with ratio $^{d}/_{a}$. These plots are generated at fixed values of ratio $^{b}/_{a}$ and the individual curves correspond to a particular value of angle α as shown in the legend. SCF remains close to 3 for the ratio $^{d}/_{a}$ closer to 10.

From these graphs, we can note maximum value of SCF decreases with decrease in angle α, increase in ratio $^{d}/_{a}$, decrease in ratio $^{b}/_{a}$. Minimum value of SCF increases with increase in angle α, decrease in ratio $^{d}/_{a}$, increase in ratio $^{b}/_{a}$. The lowest values of SCF occur (2.515) at angle $\alpha = 0°$, ratio $^{b}/_{a} = 1$ and $^{d}/_{a} = 0.4$. The highest values of SCF occur (7.61) at angle $\alpha = 89°$, ratio $^{b}/_{a} = 10$ and $^{d}/_{a} = 0.4$.

Table 1. Stress concentration factor with angle $\propto = 0°$

$^{b}/_{a}$	$^{d}/_{a}$	VGU [13]	Chiang [10]	BFM	FEM
1	1	2.658	2.625 2.623 [1] 2.650 [3]	2.602	2.682
1	2	2.787	2.703 2.703 [1] 2.715 [3]	2.675	2.752
1	3	2.864	2.772	2.746	2.813
1	4	2.907	2.825 2.825 [1] 2.827 [3]	2.798	2.863
2	1	2.556	2.924	2.991	2.961
3	1	2.404	2.982	3.019	3.021
4	1	2.255	2.993	3.001	3.035

In order to validate the results obtained from BFM, SCF values available in the literature and results of the finite element analysis (FEM) has been included in the Tables 1 and 2. Table 1 shows SCF values from [1,3,10,13] with BFM and FEM for angle $\alpha = 0°$. Computed SCF value from BFM are closer to values from [1,3,10]. SCF values from

[13] are lower than other estimation for $b > a$. Table 2 shows SCF values from [1,3,10,13] with BFM and FEM for angle $\alpha = 90°$. Computed SCF value from BFM are closer to values from [1,3,10]. SCF values from [13] are lower than other estimation for $b > a$.

Table 2. Stress Concentration factor with angle $\propto = 90°$

b/a	d/a	VGU [13]	Chiang [10]	BFM	FEM
1	1	3.97	3.264 3.264 [1] 3.264 [3]	3.242	3.316
1	2	3.481	3.066 3.066 [1] 3.066 [3]	3.092	3.108
1	3	-	3.034	3.042	3.076
1	4	3.182	3.02 3.020 [1] 3.020 [3]	3.017	3.062
2	1	3.966	4.051	3.912	4.112
3	1	3.611	4.854	4.620	4.899
4	1	3.618	5.537	5.204	5.583

Conclusions

Body Force Method is used to compute SCF around two circular holes in an infinite plate subjected to uniaxial loading along x-direction. The values of SCF obtained by using BFM closely match with the values of SCF available in the literature. BFM is simple, yet robust method useful in performing stress analysis of bodies with discontinuities. Accurate results are obtained with small number of segments of the discontinuity.

Maximum stress concentration factor is 7.61 which occurs when angle $\boldsymbol{\alpha = 89°}$, ratio of hole diameters $\boldsymbol{b/a = 10}$ and ratio of distance between holes to diameter $\boldsymbol{d/a = 0.4}$. It is found that maximum value of stress concentration factor decreases with decrease in angle α, decrease in ratio of hole diameters $\boldsymbol{b/a}$, increase in ratio of distance between holes to diameter $\boldsymbol{d/a}$.

Minimum stress concentration factor is 2.515 which occurs when angle $\boldsymbol{\alpha = 0°}$, ratio of hole diameters $\boldsymbol{b/a = 1}$ and ratio of distance between holes to diameter $\boldsymbol{d/a = 0.4}$. It is found that minimum value of stress concentration factor increases with increase in angle α, increase in ratio of hole diameters $\boldsymbol{b/a}$, decrease in ratio of distance between holes to diameter $\boldsymbol{d/a}$. The value of SCF can be maintained ≤ 3 if angle $\alpha \leq 30°$ and $b \geq 2a$.

References

1. Ling CB. On the Stresses in a Plate Containing Two Circular Holes. *J. Appl. Phys*. 1948;19(77): 77–82.
2. Davies GAO, Hoddinott JR. Stresses in a Plate Pierced by two Unequal Circular Holes. *The Journal of the Royal Aeronautical Society*. 1963;67(631): 451–452.
3. Haddon RAW. Stresses in an Infinite Plate with Two Unequal Circular Holes. *The Quarterly Journal of Mechanics and Applied Mathematics*. 1967;20(3): 277–291.
4. Salerno VL, Mahoney JB. Stress Solution for an Infinite Plate Containing Two Arbitrary Circular Holes Under Equal Biaxial Stresses. *J. Eng. Ind*. 1968;90(4): 656–665.

5. Miyata H. Finite elastic deformations of an infinite plate perforated by two circular holes under biaxial tension. *Ing. Arch*. 1970;39: 209–218.
6. Erickson PE, Riley WF. Minimizing stress concentrations around circular holes in uniaxially loaded plates. *Experimental Mechanics*. 1978;18: 97–100.
7. Iwaki T, Miyao K. Stress concentrations in a plate with two unequal circular holes. *International Journal of Engineering Science*. 1980;18(8): 1077–1090.
8. Horii H, Nemat-Nasser S. Elastic fields of interacting inhomogeneities. *International Journal of Solids and Structures*. 1985;21(7): 731–745.
9. Duan ZP, Kienzler R, Herrmann G. An integral equation method and its application to defect mechanics. *Journal of the Mechanics and Physics of Solids*. 1986;34(6): 539–561.
10. Chiang CR. A numerical method for solving elasticity problems: Application to the problems of an infinite plate containing two circular holes. *Computers & Structures*. 1988;30(5): 1199–1205.
11. Meguid SA, Gong SX. Stress concentration around interacting circular holes: a comparison between theory and experiments. *Engineering Fracture Mechanics*. 1993;44(2): 247–256.
12. Hoang SK, Abousleiman YN. Extended Green's Solution for the Stresses in an Infinite Plate with Two Equal or Unequal Circular Holes. *J. Appl. Mech*. 2008;75(3): 031016.
13. Ukadgaonker VG. *Theory of Elasticity and Fracture Mechanics*. Delhi: PHI Learning Pvt. Ltd; 2015.
14. Kuo SR, Kao SK, Huang YL, Chen JT. Revisit of the degenerate scale for an infinite plane problem containing two circular holes using conformal mapping. *Applied Mathematics Letters*. 2019;92: 99–107.
15. Zeng X, Lu A, Wang S. Shape optimization of two equal holes in an infinite elastic plate. *Mechanics Based Design of Structures and Machines*. 2020;48(2): 133–145.
16. Mohan AE, Habeeb HA, Abood AH. Experimental and modeling stress concentration factor (SCF) of a tension poly lactic acid (PLA) plate with two circular holes. *Periodicals of Engineering and Natural Sciences*. 2019;7(4): 1733–1742.
17. Gandilyan DV, Ustinov KB. Influence of surface effects on stress state in a body with two circular holes. *J. Phys.: Conf. Ser*. 2020; 1474: 012014.
18. Patel A, Desai CK. Stress concentration around an elliptical hole in a large rectangular plate subjected to linearly varying in-plane loading on two opposite edges. *Theoretical and Applied Fracture Mechanics*. 2020;106: 102432.
19. Yang L, Wang Q, Xu L, Yang R, Chao YJ. Fracture path of cracks emigrating from two circular holes under blasting load. *Theoretical and Applied Fracture Mechanics*. 2020;108: 102559.
20. Ma Y, Lu A, Cai H, Zeng X. An analytical method for determining the plastic regions around two circular holes in an infinite medium. *Applied Mathematical Modelling*. 2021;89(1): 636–653.
21. Maksymovych M, Lazorko A, Maksymovych O, Dmitriiev O. Research of Stress Concentration at Closely Placed Holes in Wing Bearing Area in Anisotropic Platesю *Diagnostyka*. 2022;23(4): 2022402.
22. Nisitani H. Solutions of notch problems by body force method. In: Sih GC. (ed.) *Mechanics of Fracture, Volume 5*. Alphen aan den Rijn: Noordhoff Intern Publ.; 1978. p.1–68.
23. Nisitani H, Saimoto A. Short History of Body Force Method and its Application to Various Problems of Stress Analysis. *Materials Science Forum*. 2003;440–441: 161–168.
24. Chen D, Nisitani H. Body force method. *International Journal of Fracture*. 1997;86: 161–189.
25. Fraga WE, Hewitt RL. *Implementation of Nisitani's Body Force Method for the Solution of Notch Problems*. National Aeronautical Establishment, NAE-AN-17, NRC NO. 22831 Ottawa; 1983.

About Author

Shrikrishna M. Badiger
Assistant Professor (M.S. Ramaiah University of Applied Sciences, Bengaluru, India)

Daivajna Subbarayappa Ramakrishna
PhD, Professor (Jawaharlal Nehru National College of Engineering, Shivamogga, India)